STEM CELLS®

TISSUE-SPECIFIC STEM CELLS

Subventricular Zone Localized Irradiation Affects the Generation of Proliferating Neural Precursor Cells and the Migration of Neuroblasts

PRAGATHI ACHANTA,[a] VIVIAN CAPILLA-GONZALEZ,[a] DAVID PURGER,[a] JUVENAL REYES,[c] KURT SAILOR,[d] HONGJUN SONG,[d] JOSE MANUEL GARCIA-VERDUGO,[b] OSCAR GONZALEZ-PEREZ,[e] ERIC FORD,[c] ALFREDO QUINONES-HINOJOSA[a]

[a]Department of Neurosurgery, [c]Department of Radiation Oncology and Molecular Radiation Sciences, and [d]Institute for Cell Engineering, Johns Hopkins University School of Medicine, Baltimore, Maryland, USA; [b]Laboratory of Comparative Neurobiology, Instituto Cavanilles, University of Valencia, Valencia, CIBERNED, Spain; [e]Laboratory of Neuroscience, Facultad de Psicologia, Universidad de Colima, Colima, Mexico

Key Words. Radiation therapy • Neural stem cells • Migrating neuroblasts • Subventricular zone

ABSTRACT

Radiation therapy is a part of the standard treatment for brain tumor patients, often resulting in irreversible neuropsychological deficits. These deficits may be due to permanent damage to the neural stem cell (NSC) niche, damage to local neural progenitors, or neurotoxicity. Using a computed tomography-guided localized radiation technique, we studied the effects of radiation on NSC proliferation and neuroblast migration in the mouse brain. Localized irradiation of the subventricular zone (SVZ) eliminated the proliferating neural precursor cells and migrating neuroblasts. After irradiation, type B cells in the SVZ lacked the ability to generate migrating neuroblasts. Neuroblasts from the unirradiated posterior SVZ did not follow their normal migratory path through the irradiated anterior SVZ. Our results indicate that the migrating neuroblasts were not replenished, despite the presence of type B cells in the SVZ post-irradiation. This study provides novel insights into the effects of localized SVZ radiation on neurogenesis and cell migration that may potentially lead to the development of new radiotherapy strategies to minimize damage to NSCs and neuroblast migration. STEM CELLS *2012;30:2548–2560*

Disclosure of potential conflicts of interest is found at the end of this article.

INTRODUCTION

Brain irradiation is an integral component of the treatment of patients with brain tumors [1, 2]. Despite its effectiveness in controlling the progression of some cancers, radiation is often associated with neuropsychological deficits [3–6]. These deficits may be partly due to radiation-induced damage to neurogenic niches, as shown in animal models [7–11]. In the adult mammalian brain, these niches are localized in the subventricular zone (SVZ) and the subgranular zone of the hippocampal dentate gyrus [12–14]. The neural stem cells (NSCs) in these two regions are of great interest for therapeutic applications in the brain because of their ability to proliferate and produce new cells. These newly generated cells are able to migrate and differentiate into any of the main cell types of the central nervous system, such as neurons, oligodendrocytes, or astrocytes [12–15]. Damaging NSCs during radiation therapy can have detrimental effects [4, 7]. Mitigating the neurotoxic effects of radiation is important particularly in the context of brain tumor patients who survive longer due to new combination therapies [1, 2, 6]. Furthermore, NSCs have the potential to be used to treat brain cancer in two different ways. First, endogenous NSCs in the brain can participate in the repair of normal tissue and/or inhibit tumor growth [16]. Second, engineered stem cells may be used to deliver cytotoxic agents and prodrug-activating enzymes to the tumor [17–21]. Both of these possibilities require that NSCs generate neuroblasts to migrate toward the tumor site, a process that is not well-understood in the context of radiation therapy.

The SVZ is the largest source of NSCs in the adult brain, located underneath the layer of ependymal cells lining the

Author contributions: P.A.: conception and design of experiments, data collection, assembly, analysis and interpretation, manuscript writing, final approval of manuscript, and contributed to the manuscript editing; D.P.: data collection, assembly, analysis, and contributed to the manuscript editing; J.R.: data collection and contributed to the manuscript editing; V.C.G. and J.M.G.V.: data collection, assembly, analysis and interpretation from electron microscopy, and contributed to the manuscript editing; K.S. and H.S.: provided the GFP expressing retrovirus, assisted with stereotactic injections, and contributed to the manuscript editing; O.G.P.: experimental design, data interpretation, and contributed to the manuscript editing; E.F.: conception and design of experiments, SARPP technology, data interpretation, and contributed to the manuscript editing; A.Q.H.: conception and design of experiments, final approval of manuscript, financial support, and contributed to the manuscript editing.

Correspondence: Alfredo Quinones-Hinojosa, M.D., Department of Neurosurgery, Johns Hopkins University, 1550 Orleans St, CRB-II, Room 247, Baltimore, Maryland 21201, USA. Telephone: 410-502-2869; Fax: 410-502-7559; e-mail: aquinon2@jhmi.edu Received April 13, 2012; accepted for publication July 21, 2012; first published online in STEM CELLS *EXPRESS* September 4, 2012. 1066-5099/2012/$30.00/0 doi: 10.1002/stem.1214

ventricles [13, 22–24]. NSCs, or type B1 cells in the SVZ, are astrocyte-like glial fibrillary acidic protein ($GFAP^+$) cells that divide and give rise to transit amplifying neural precursor cells (NPCs), or type C cells, which in turn give rise to migrating neuroblasts, or type A cells [25]. Neuroblasts migrate long distances through the rostral migratory stream (RMS) before differentiating into olfactory bulb (OB) interneurons [26, 27]. The mouse SVZ-RMS-OB migration route represents a well-characterized system of endogenous neuroblast migration that serves as a model to study migration in humans receiving radiotherapy [27, 28].

Current radiotherapy treatments, such as intensity-modulated radiation therapy, are intended to deliver a maximum dose of radiation to the tumor while reducing radiation exposure to the surrounding normal tissue [29, 30]. To more accurately reproduce human radiotherapy, we used a small animal radiation research platform (SARRP) developed in-house [31]. Using this technology, we recently reported that local irradiation of hippocampus significantly decreased the number of proliferating cells in the irradiated dentate gyrus compared to the unirradiated side [32]. Furthermore, the number of newborn cells differentiating into mature neurons 2 months after irradiation was significantly reduced [32]. In this study, we examined the effect of SVZ-restricted irradiation on NSC and NPC proliferation and neuroblast migration in the adult mouse SVZ-RMS-OB system. The two main findings from this study are that type B cells lacked the ability to regenerate NPCs and neuroblasts even a month after irradiating SVZ, and that neuroblasts failed to migrate through the irradiated regions. These results will help inform future radiotherapy protocols to minimize damage to neurogenic niches in the human brain.

Materials and Methods

Subjects

The subjects were 6–8-week-old male C57BL6/J mice from the National Cancer Institute maintained on a 12:12 hour light/dark cycle. Food and water were available ad libitum. All experiments described were performed with the approval of the Johns Hopkins Animal Care and Use Committee under standard protocols.

Computed Tomography-Based Localized Brain Irradiation

Mice were anesthetized with the injection of 100 mg/kg ketamine + 10 mg/kg xylazine intraperitoneally. To directly visualize the ventricles and target the SVZ, 70 μl of iodine contrast was injected intrathecally and computed tomography (CT) images were obtained as described previously [32]. A single dose of 10 Gy was delivered using CT-based tissue visualization. Previous studies have demonstrated that the overall geometric targeting accuracy of this technique is 0.2 mm [32]. A radiation beam of 3×3 mm^2 was used to target right SVZ while left brain structures served as controls. For migration studies, a radiation beam of 1-mm diameter was used to target the anterior dorsal region of the SVZ. Additionally, a radiation beam of 5×9 mm^2 was used to target right OB, RMS, and/or anterior SVZ (aSVZ). For sham irradiation, control animals were anesthetized, brought into the treatment room, and handled and positioned identically to irradiated animals without radiation delivery.

Immunohistochemistry

Mice ($n = 5$ per group) were deeply anesthetized and perfused transcardially with 0.9% saline followed by 4% paraformaldehyde (PFA) in 0.1 M phosphate-buffered saline (PBS). Brains were removed from the skull and postfixed in 4% PFA overnight at 4°C. The brains were then equilibrated in 30% sucrose and were frozen in Tissue-Tek OCT Compound. Ten-micrometer-thick coronal slices were sectioned using a cryostat. Sections were treated with 0.01 M sodium citrate at 95°C for 10 minutes for antigen retrieval. Sections were incubated in PBS containing 0.1% Triton X-100, and 10% normal goat serum (NGS) for 30 minutes, and then incubated with primary antibodies for 16 hours at 4°C. Primary antibodies used in this study were mouse anti-rH2Ax (Ser139) (1:700), rabbit anti-Ki67 (1:200), mouse anti-GFAP (1:500), rabbit anti-doublecortin (DCx) (1:500), mouse anti-nestin (1:100), mouse anti Mash-1 (1:100), cleaved caspase-3 (1:100), and mouse anti-CD31 (1:200). More details on the primary antibodies are summarized in supporting information Table S1. The sections were washed with PBS and incubated with secondary antibodies conjugated with fluorophores for 1 hour at room temperature (RT). Anti-mouse, anti-rat, and anti-rabbit Alexa 488 and/or 594 secondary antibodies (1:500; Invitrogen, Green Island, NY, USA) were used. Nuclei were stained with 4',6-diamidino-2-phenylindole (DAPI) (1:500) All the sections were air-dried and coverslipped with .Aquamount mounting media (Vector Labs, Burlingame, CA, USA). Fluorescent images were taken with an ORCA II camera (Hamamatsu) connected to an Olympus IX81 inverted microscope.

SVZ Whole Mount Dissection and Immunostaining

Mice ($n = 3$ per group) were sacrificed by cervical dislocation and their brains were immediately extracted into L-15 Leibovitz medium (Gibco, Green Island, NY, USA). A whole mount of SVZ tissue (2–4 mm) with the lateral ventricle and striatum was dissected under microscope, and the hippocampus and septum were removed as described [24, 33]. The SVZ whole mounts were fixed in 4% PFA/0.1% Triton X-100 overnight at 4°C. They were then washed with PBS and blocked with 10% NGS/0.5% Triton for 30 minutes at RT. The tissues were incubated in primary and secondary antibodies diluted in blocking buffer for 48 hours at 4°C. After staining, the SVZ whole mounts were further dissected from underlying striatum to 200–300-μm thick tissue, transferred to a glass slide, and coverslipped with Aquamount mounting media for imaging. A Nikon C1si True Spectral Imaging Confocal Laser Scanning Microscope was used to image the SVZ whole mounts.

Semithin Sections, Electron Microscopy, and Ultrastructural Analysis

Mice ($n = 5$ per group) were anesthetized and perfused with 0.9% saline, followed by 2% PFA and 2.5% glutaraldehyde. Heads were removed and postfixed in the same fixative overnight. After postfixation, brains were dissected and washed in 0.1 M phosphate buffer (PB) (pH 7.4), cut into 200 μm coronal sections with a VT 1000M vibratome (Leica, Wetzlar, Germany), and treated with 2% osmium tetraoxide in 0.1 M PB for 2 hours. Sections were then rinsed, dehydrated through increasing ethanol solutions, and stained with 2% uranyl acetate in 70% ethanol. Following dehydration, slices were embedded in araldite (Durcupan, Fluka BioChemika, Ronkokoma, NY). To study the cellular organization of the SVZ and RMS, we cut serial 1.5 μm coronal semithin sections with a diamond knife and stained them with 1% Toluidine blue. Sections were visualized under E200 light microscope (NIKON, Tokyo, Japan). To identify cell types, 60–70 nm ultrathin sections were cut with a diamond knife, stained with lead citrate, and examined under a Spirit transmission electron microscope (FEI Tecnai, Hillsboro, OR). The different cell types in the SVZ and RMS were identified based on their ultrastructural characteristics as described previously [25].

SVZ Neurosphere Cultures

Adult mouse brains were removed into sterile cold Neurocult basal medium (Stem Cell Technologies, Vancouver, BC,

Canada). The SVZ was dissected out from each hemisphere as described in Ferron et al. [34]. The left and right SVZ were collected separately and pooled from four different mice. The tissue was triturated gently until all the pieces were dissociated and cell suspension was homogenous. The cells were washed in the complete mouse Neurocult proliferation medium with Neurocult proliferation supplement, recombinant growth factors (10 μg/ml epidermal growth factor and 10 μg/ml fibroblast growth factor), and 2 μg/ml heparin (Stem Cell Technologies, Vancouver, BC, Canada). Viable cells were counted and plated at 2×10^4 cells per square centimeter. The cultures were incubated at 37°C in a 5% CO_2 humidified incubator adding fresh medium every 4 days. Neurospheres of 100–200 μm size were passaged and replated.

Retrovirus Preparation and Stereotactic Injections

Engineered self-inactivating murine oncoretrovirus expressing green fluorescent protein (GFP), with the Woodchuck hepatitis virus post-transcriptional regulatory element under the Ubiquitin-C promoter, was produced as previously described [35]. A day after irradiation, mice ($n = 5$ per group) were anesthetized with ketamine (100 mg/kg)/xylazine (10 mg/kg) anesthesia and injected with buprenorphine (0.02 mg/kg) for postoperative analgesia. The head was secured to a stereotaxic frame (David Kopf, Tujunga, CA, USA). The skull surface was exposed and retrovirus was injected (1 microliter per site) into the SVZ using a glass needle at the following two different coordinates bilaterally relative to bregma: anterior = 1.0 mm, lateral = ±1.0 mm, ventral = 2.2 mm; anterior = 0. 0 mm, lateral = ±1.8 mm, ventral = 1.6 mm. The scalp was sutured and the mice were returned to their standard housing. Mice were sacrificed a week after retrovirus injections, the brains were fixed, sectioned sagittally, and immunostained against Ki67. Sections were visualized under a microscope for GFP-expressing migrating neuroblasts and $Ki67^+$ cells. The experimental paradigm is shown in Figure 7A.

Cell Quantification and Statistical Analysis

In the coronal sections of the mouse brain, the quantification of $Ki67^+$ cells in the SVZ, RMS, and OB was performed on every 20th section evenly spaced along the entire rostral-caudal length of the lateral ventricle of the SVZ using a fluorescent microscope. A total of 7, 9, and 10 sections were counted for SVZ, RMS, and OB, respectively, for each animal. The cell counts for all mice in a given group were averaged per section and the SEM was calculated. To quantify the number of cells within the SVZ under electron microscope, we considered the area comprised of the first 20 μm adjacent to the ventricle lumen (0–1 mm anterior to bregma). The counts were performed on three different levels per animal, and the average was shown in cells per mm. Blood vessel analysis was performed using semithin sections. We considered the area comprising the first 100 μm adjacent to the ventricle lumen (0–1 mm anterior to bregma). The number and size of blood vessels were measured with Image Tool software (Evans Technology, Roswell, Georgia). Changes in RMS size were determined by measuring the area occupied by RMS in semithin sections using a light microscope, at three different levels per animal. The analysis was performed with Image Tool software. An unpaired t test was performed using SigmaPlot 11.0 software (Systat Software Inc, San Jose, CA) to determine the difference between the left and right SVZ for all our data quantified. The differences were considered significant at a p-value less than .05.

Results

Localized Radiation Eliminates Actively Proliferating Cells in the SVZ

A series of pilot experiments was performed to validate the localized nature of the radiation beams from the SARRP. A 10-Gy, 3×3 mm^2 field of localized radiation was delivered to the right ventricle while the nonirradiated left ventricle served as a control (Fig. 1A). The accuracy of localized radiation delivery in the targeted right SVZ region was validated by immunohistochemical staining of γH2Ax, a marker of DNA double-strand breaks, 1 hour post-irradiation. The irradiated right ventricle of the mouse brain showed restricted expression of γH2Ax (Fig. 1B). Cell proliferation in the SVZ was assessed by immunostaining against Ki67 in response to the localized radiation. A strong lateral asymmetry in cell proliferation was observed on every coronal section 1-day post-irradiation (Fig. 1C) and on SVZ whole mounts 1-month post-irradiation (Fig. 1D). There was a significant decrease in the number of $Ki67^+$ cells in the right SVZ at 1 day (left SVZ: 85.05 ± 12.84 cells per section vs. right SVZ: 14.27 ± 2.35 cells per section) (Fig. 1E) and 1 month (left SVZ: 56 ± 5.26 cells per section vs. right SVZ: 7 ± 1.67 cells per section) (Fig. 1F) after irradiation ($p < .001$). Remarkably, the number of proliferating cells in the RMS and OB was not affected by localized radiation of the SVZ at either 1 day or 1 month after irradiation (Fig. 1E, 1F). These results indicate that the vast majority of proliferating cells in the mouse SVZ were permanently eliminated in a highly localized fashion using SARRP technology.

Localized Radiation of SVZ Decreases NPCs and Neuroblasts

We then explored the effect of localized radiation on different cell types in the SVZ, such as NSCs/type B1 cells, NPCs/type C cells, and migrating neuroblasts/type A cells, using cell specific markers and electron microscopy 1-month post-irradiation. Nestin and GFAP immunostaining was used to label type B cells, Mash-1 for type C cells, and DCx for migrating neuroblasts [24]. While GFAP and nestin expression appeared to remain stable (Fig. 2A, 2C), there was a strong qualitative reduction of $Mash\text{-}1^+$ cells (Fig. 2B) and DCx^+ cells (Fig. 2C). The $GFAP^+$ type B1 cells in the coronal sections were distinguished by their contact with the ventricular surface (arrowheads in Fig. 2A) and long distal processes (arrows in Fig. 2A) from the parenchymal astrocytes or type B2 cells that form glial tubes and are also positive for GFAP [24]. GFAP and DCx costaining of lateral ventricle whole mounts further confirmed the presence of $GFAP^+$ cells and the absence of DCx^+ cells in the irradiated SVZ (Fig. 2D). These findings from SVZ immunostaining were further confirmed with electron microscopy, and quantitative analysis of different cell types was performed using electron microscopy (Fig. 3).

Light and electron microscope examination of the SVZ showed a clear disruption in both the antero-posterior and dorso-ventral axes in irradiated hemisphere 1 month after irradiation. While the cell organization in nonirradiated SVZ appeared normal, with a monolayer of ependymal cells and typical chains of migratory neuroblasts (dark cells) surrounded by type B cells (light cells), SVZ in irradiated hemisphere was reduced to ependymal cells with dispersed astrocytes and neuronal bodies close to the ventricle (Fig. 3A, 3C). There were no migratory chains after irradiation (Fig. 3A, 3C), but dispersed type A cells were occasionally observed. Consequently, cell density was drastically decreased in irradiated SVZ (left SVZ: 236.1 ± 26.2 cells per mm vs. right

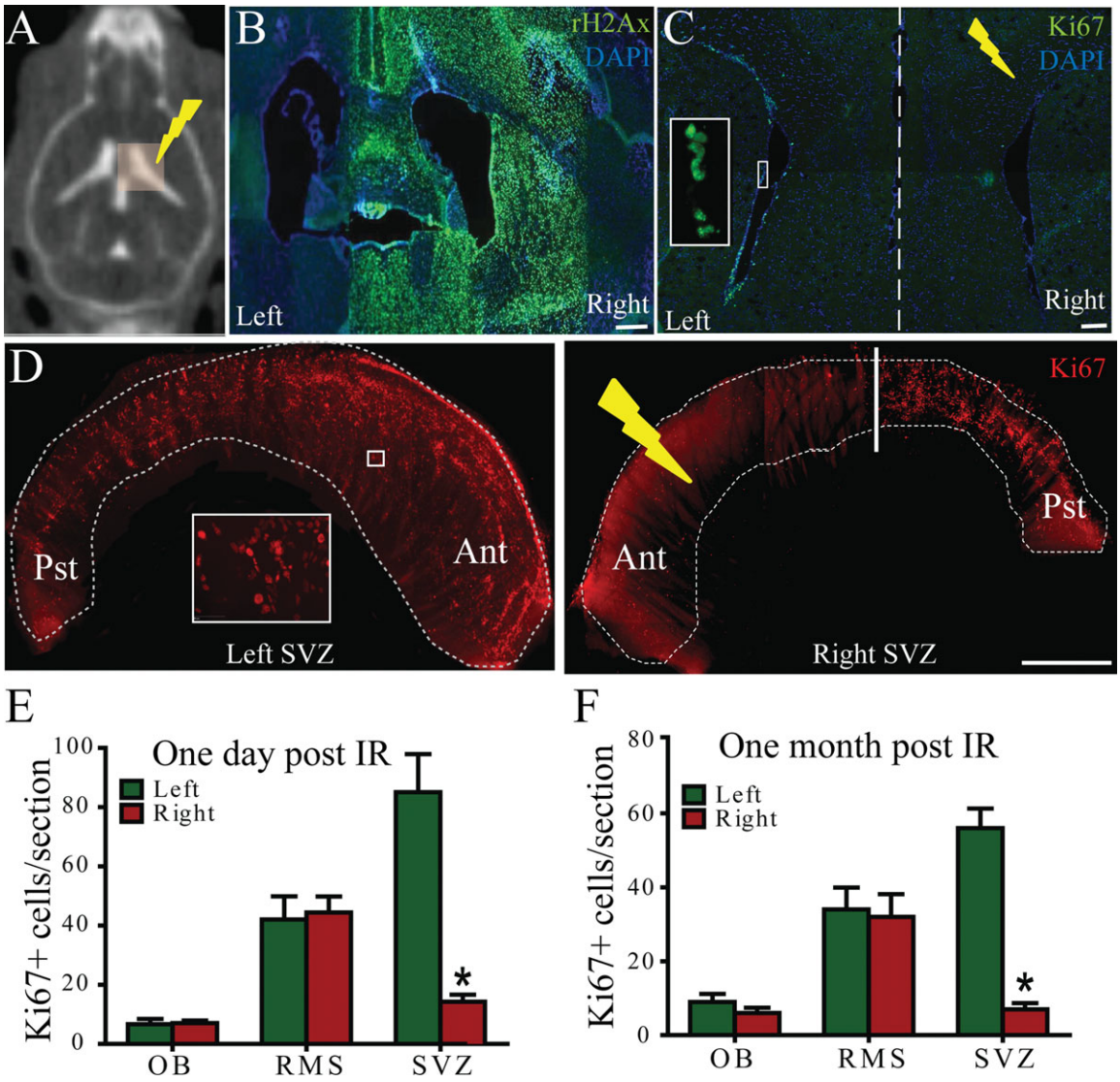

Figure 1. Localized radiation of the right SVZ disrupts proliferation as compared to the left (control) side. **(A):** Computed tomography image of a mouse after intrathecal iodine contrast showing ventricles and radiation plan with 3 × 3 mm^2 beam covering the right ventricle. **(B):** Immunohistochemistry (IHC) against γH2Ax (green) 1 hour after radiation confirmed that the 3 × 3 mm^2 beam irradiated only the right lateral ventricle. **(C):** IHC against Ki67 of a coronal section of the mouse brain 1 day post-irradiation. Inset shows the $Ki67^+$ cells (green) at higher magnification. **(D):** Whole mount staining of SVZ against Ki67 1 month post-irradiation. Inset shows the $Ki67^+$ cells (red) at higher magnification. The number of $Ki67^+$ cells in the irradiated SVZ decreased significantly compared to the control SVZ after 1 day **(E)** and 1 month **(F)**. Scale bars = 100 μm (B, C), 1 mm (D). *, $p < .001$. Abbreviations: Ant, anterior; DAPI, 4',6-diamidino-2-phenylindole; OB, olfactory bulb; Pst, posterior; RMS, rostral migratory stream; SVZ, subventricular zone.

SVZ: 97.9 ± 6 cells per mm; $p < .005$) (Fig. 3B). This loss of cell density was attributed to a decrease in the number of type B cells (left SVZ: 76.8 ± 7.2 cells per mm vs. right SVZ: 38.2 ± 6.6 cells per mm; $p = .004$), type C cells (left SVZ: 25.5 ± 5.9 cells per mm vs. right SVZ: 0.5 ± 0.3 cells per mm; $p = .01$), and type A cells (left SVZ: 77.0 ± 17.0 cells per mm vs. right SVZ: 3.5 ± 0.6 cells per mm; $p = .01$), while ependymal cells remained unaltered (left SVZ: 46.9 ± 2.9 cells per mm vs. right SVZ: 46.8 ± 2.3 cells per mm) (Fig. 3D and supporting information Table S2). Most importantly, type B1 cells, identified by their apical process extending into the lateral ventricle and primary cilia, were observed in the right SVZ 1 month after irradiation (Fig. 3E, 3E′, and Table 2). Extensive portions of basal lamina were found frequently between astrocytes and/or ependymal cells in the irradiated SVZ, compared to nonirradiated hemisphere (Fig. 3F). As a result of the decreased cell density, neuropil structures were shifted medially toward the ependymal layer in the right SVZ following irradiation. Mylenic and amylenic axons, including synaptic contacts, were observed adjacent to the ependymal layer, establishing direct contact with ependymal and/or astrocytic cells in some cases (Fig. 3G). Together, these results indicate that the migrating neuroblasts were not replenished even 1 month after irradiation, despite the presence of type B cells in the SVZ post-irradiation (Figs. 2, 3E).

Localized Radiation Affects the Generation of NPCs and Migrating Neuroblasts from NSCs

The presence of type B1 cells after irradiation raised the question if their proliferation was intact. Double labeling of the SVZ against nestin and Ki67 1 month after radiation showed proliferation in few of the residual type B cells (Fig. 4A). These proliferating type B cells were further found to be in proximity

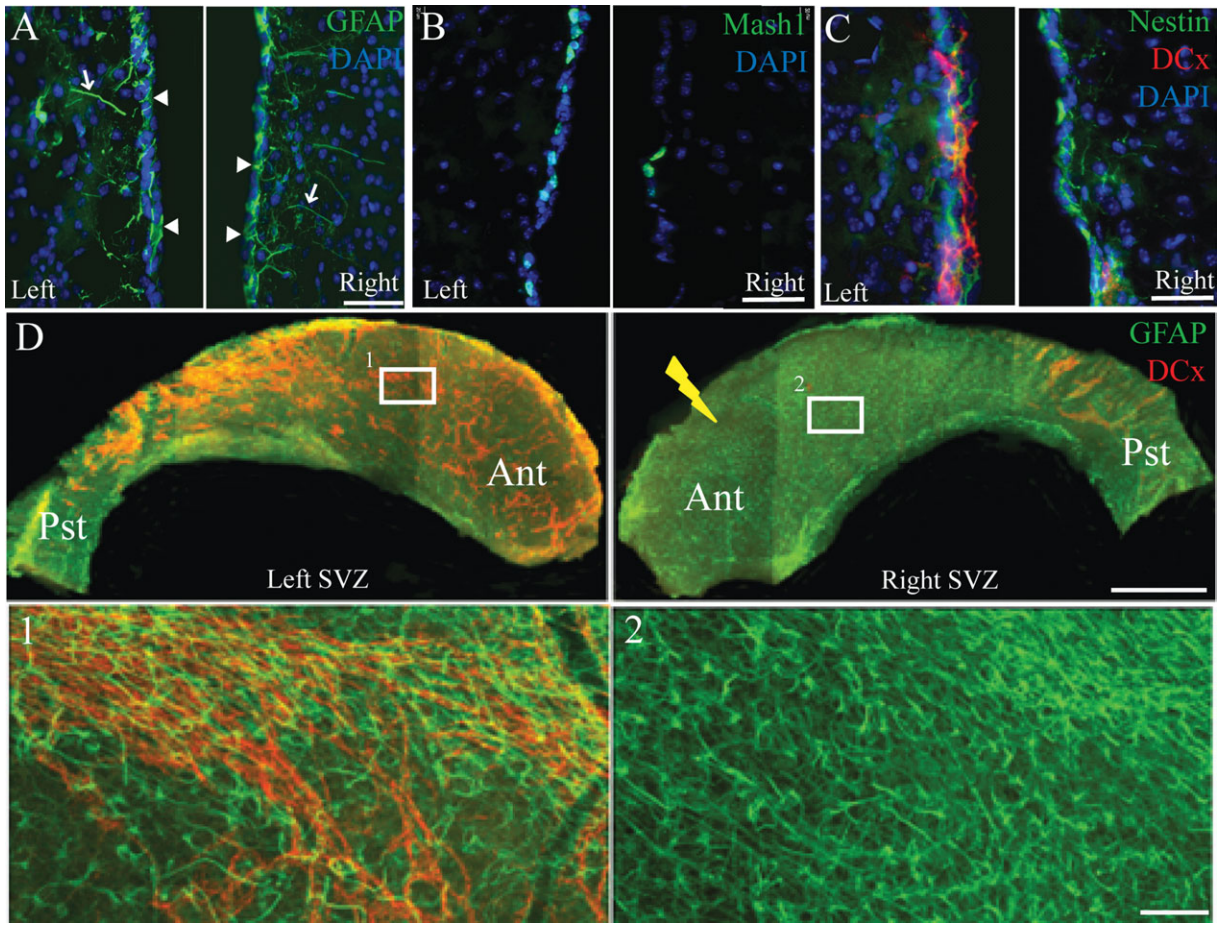

Figure 2. Localized irradiation of the right SVZ eliminates the neural precursor cells (NPCs) and migrating neuroblasts but not type B cells after 1 month. **(A):** GFAP$^+$ cells (green) in a coronal section of the mouse brain appeared to show no difference between the left and right SVZ. Type B cells were identified by their long GFAP processes (arrows) and their contact with the lateral ventricle (arrowheads). **(B):** Fewer Mash-1$^+$ NPCs (green) in the right SVZ with localized radiation compared to the control left SVZ. **(C):** Nestin (green) and DCx (red) double labeling showed the presence of type B cells but not migrating chains of neuroblasts upon localized radiation. **(D):** GFAP (green) and DCx (red) immunohistochemistry of whole mount SVZ also confirmed the ablation of neuroblasts after localized radiation (right SVZ) after 1 month. Higher magnification images of left and right whole mount SVZ (insets) are shown in 1 and 2. Scale bars = 50 μm (A--C), 1 mm (D), 100 μm (insets 1 and 2). Abbreviations: Ant, anterior; DAPI, 4',6-diamidino-2-phenylindole; DCx, doublecortin; GFAP, glial fibrillary acidic protein; Pst, posterior; SVZ, subventricular zone.

to blood vessels (Fig. 4B). CD31 immunostaining for endothelial cells in the SVZ appeared to be no different between the control and irradiated SVZ (supporting information Fig. S1A). These results were also confirmed by electron microscopy, where the basal lamina and endothelial cells were no different between the left (unirradiated) SVZ and the right (irradiated) SVZ (supporting information Fig. S1B). There was no difference in the number of blood vessels (left SVZ: 66 $\pm$ 4.93 vs. right SVZ: 51 $\pm$ 7.57; $p = .172$) and in the size of the blood vessels (left SVZ: 50.93 $\pm$ 11.6 vs. right SVZ: 45.09 $\pm$ 7.29; $p = .692$) as quantified in the semithin section (supporting information Fig. S1C, S1D). Interestingly, when the dissected SVZ tissue was dissociated and cultured in vitro, the cells from the left SVZ gave rise to neurospheres, whereas the cells from the irradiated right SVZ failed to form neurospheres (Fig. 4C). Taken together, these results indicate that the residual type B cells are able to proliferate after irradiation but lack the ability to generate NPCs and migrating neuroblasts.

Localized Radiation of SVZ Affected the Size of the RMS

Although there was no significant difference in the number of proliferating cells in the RMS (Fig. 1F), there were fewer DCx$^+$ migrating neuroblasts in the right RMS 1 month after localized right SVZ radiation as compared to the left RMS (Fig. 5B). In addition, there was a significant reduction in cross-sectional size of the RMS (left RMS: 9,892 $\pm$ 737 mm^2 vs. right RMS: 7,202 $\pm$ 474 mm^2) (Fig. 5C). Ultrastructural analysis with electron microscopy revealed no morphological alterations in cell populations of the RMS despite the reduction in size (Fig. 5D). Furthermore, we noticed few cells in the irradiated RMS in their mitotic phase, which based on their ultrastructural features, were identified as neuroblasts (Fig. 5D, inset).

Localized Radiation Disrupts the Migration of Neuroblasts

The anterior dorsal SVZ is one of the regions with the largest NSC population [24]. In this experiment, we irradiated the anterior dorsal region of the SVZ with a single 10-Gy lateral beam of 1-mm diameter (supporting information Fig. S2A, S2B). Whole mount staining of SVZ against GFAP and DCx showed no neuroblasts in the irradiated region after 1 week (supporting information Fig. S2C). Additionally, no neuroblasts from the posterior dorsal SVZ were found to migrate into the irradiated region indicating that radiation may have affected the migration of neuroblasts in the SVZ (supporting information Fig. S2C′, S2C″). We then examined the effect of

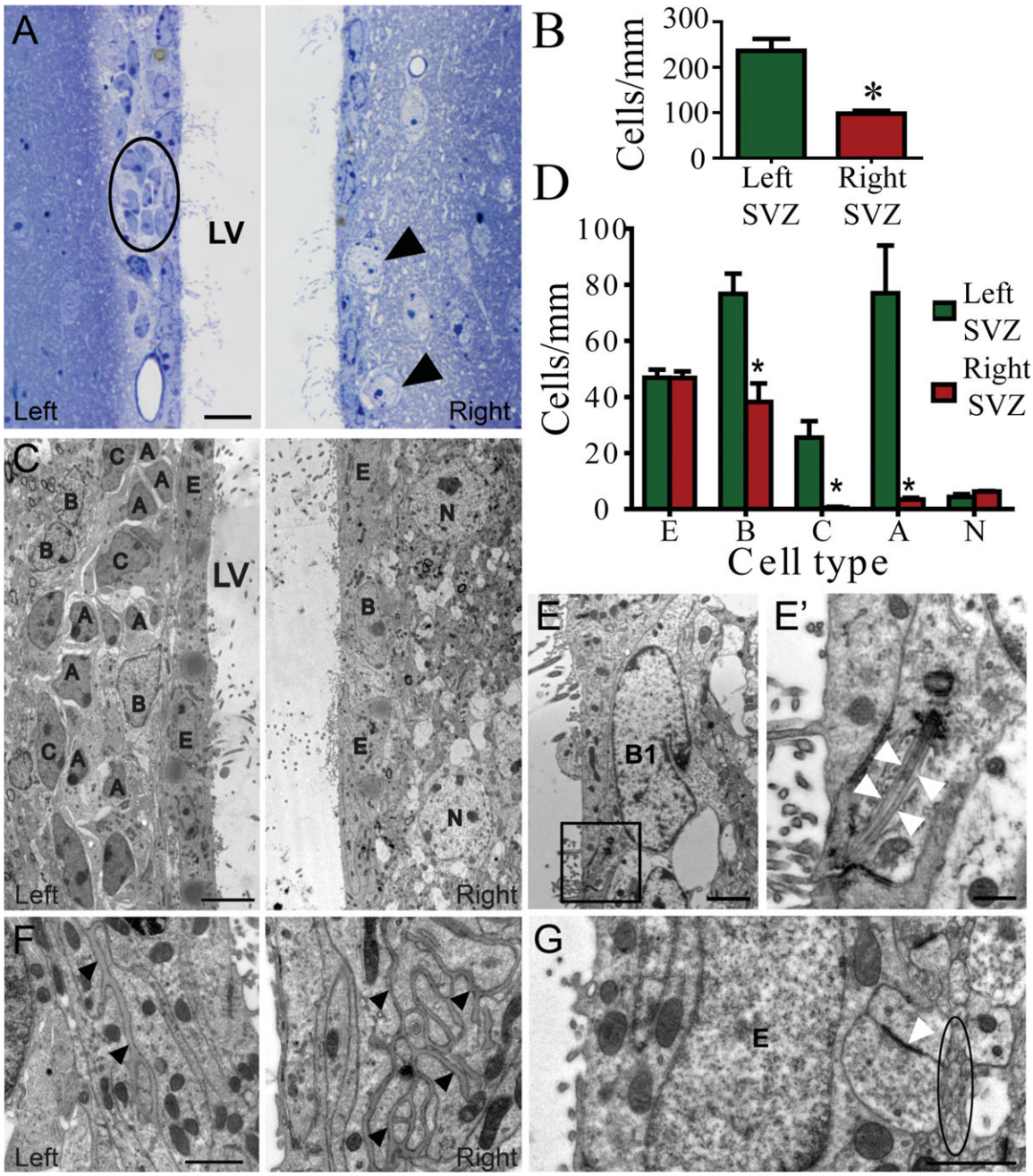

Figure 3. Cell organization of the nonirradiated left and irradiated right SVZ 1 month post-irradiation. **(A):** Semithin sections of the left SVZ reveal typical cell organization with dark cells forming the migratory chains (circle) surrounded by expansions of astrocytes (light cells), located beneath the ependymal layer, while the irradiated SVZ lacks the proliferative populations, showing a monolayer of ependymal cells with neurons located close to the ventricle (arrow). **(B):** Bar graph representing the number of cells per mm for the total cells in the SVZ, resulting in a cell reduction in the irradiated hemisphere. **(C):** Electron micrographs depict details of each cell type remained in the left and right SVZ. Irradiated SVZ was reduced to a monolayer of ependymal cells with dispersed astrocytes and neurons without neural precursor cells or neuroblasts. **(D):** Bar graph representing the number of cells per mm for each SVZ cell type. **(E):** Electron micrograph of a B1 cell contacting the lumen of the lateral ventricle of irradiated SVZ. Details of the primary cilia are shown at higher magnifications (**E′** arrowheads). **(F):** Basal lamina in the right SVZ was more extensive after irradiation compared to the left SVZ (arrowheads). **(G):** Amyelenic axons (circle) and synaptic contacts (arrowheads) next to ependymal cells in contact with ependymal cells in the irradiated SVZ. Scale bars = 10 μm (A), 5 μm (C), 2 μm (E), 500 nm (E′), 1 μm (F, G). *, $p <$ .001. Abbreviations: A, neuroblast; B, astrocyte; BV, blood vessel; C, type C cell; LV, lateral ventricle; N, neuron; SVZ, subventricular zone.

irradiation on anterior SVZ (aSVZ) while sparing the posterior SVZ. A 5 $\times$ 9 mm^2 beam of 10 Gy was used to deliver radiation to the aSVZ, RMS, and OB (Fig. 6A). Immunostaining of SVZ whole mount against γH2Ax, 1-hour post-irradiation, showed a precise radiation field confined only to the aSVZ, sparing the posterior SVZ (Fig. 6B). DCx$^+$ neuroblasts were seen 1 hour post-irradiation, but were absent after 1 day and 1 month post-irradiation (Fig. 6C). The neuroblasts from the posterior SVZ did not migrate through the irradiated aSVZ, consistent with our results in supporting information Figure S2. Furthermore, there were no apoptotic cells observed 1 week after localized irradiation of the

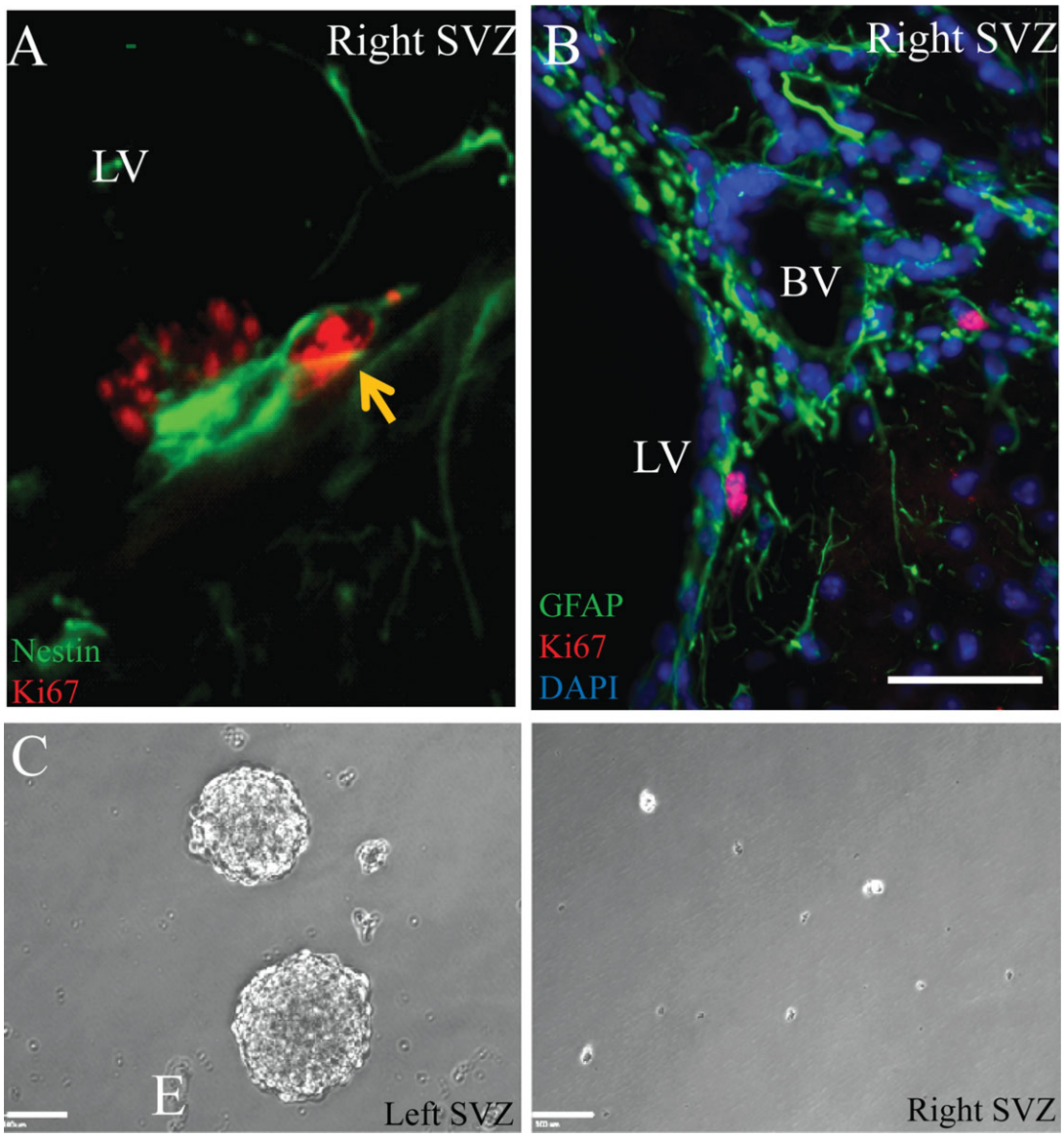

Figure 4. Residual type B cells in the irradiated right SVZ 1 month after radiation. **(A):** Nestin (green) and Ki67 (red) double labeling show proliferating type B cells in the right SVZ (arrow). **(B):** GFAP (green) and Ki67 (red) show proliferating type B cells (arrow) in proximity to blood vessels. **(C):** Neurospheres were formed from unirradiated control SVZ (left), while no neurospheres were formed from the 10-Gy-irradiated SVZ (right). Scale bars = 50 μm (B), 100 μm (C). Abbreviations: BV, blood vessel; DAPI, 4',6-diamidino-2-phenylindole; GFAP, glial fibrillary acidic protein; LV, lateral ventricle; SVZ, subventricular zone.

anterior SVZ, as assessed by immunohistochemistry against activated Caspase-3 (data not shown).

To evaluate whether the migratory properties of neuroblasts were affected by irradiation, we injected GFP-expressing retrovirus into the SVZ to label NSCs and track the migratory pattern of newly generated neuroblasts, 1 day after radiation treatment. Three separate groups of mice received either no radiation or a single 10-Gy dose to their RMS/OB (sparing the entire SVZ) or to their aSVZ/RMS/OB. One day after irradiation, mice were injected with GFP-expressing retrovirus in the SVZ to label dividing NSCs and track the migration of neuroblasts (Fig. 7A). As predicted, sham-irradiated mice had GFP^+ cells in the SVZ, RMS, and OB 1 week after injection (Fig. 7B, insets 1–4). Mice that received radiation to the RMS/OB showed GFP^+ cells in their SVZ but not in RMS and OB (Fig. 7C, inset 5). Mice that received radiation to the aSVZ/RMS/OB showed no GFP^+ cells (Fig. 7D). Quantification of $Ki67^+$ cells further revealed that the RMS/OB irradiation did not affect the SVZ proliferation (supporting information Fig. S3). These results indicate that irradiation of the RMS alone (sparing SVZ) can inhibit the migration of neuroblasts. Our findings suggest that irradiation did not disrupt the intrinsic mechanism of neuroblast migration, but the local microenvironment permissive of cell migration.

Discussion

The effect of radiation on NSC/NPC proliferation and neuroblast migration cannot be disregarded, given that radiation therapy is a first-line treatment for many brain tumors, including glioblastoma [2]. Numerous studies have examined the decrease in proliferating cells in SVZ and subgranular zone

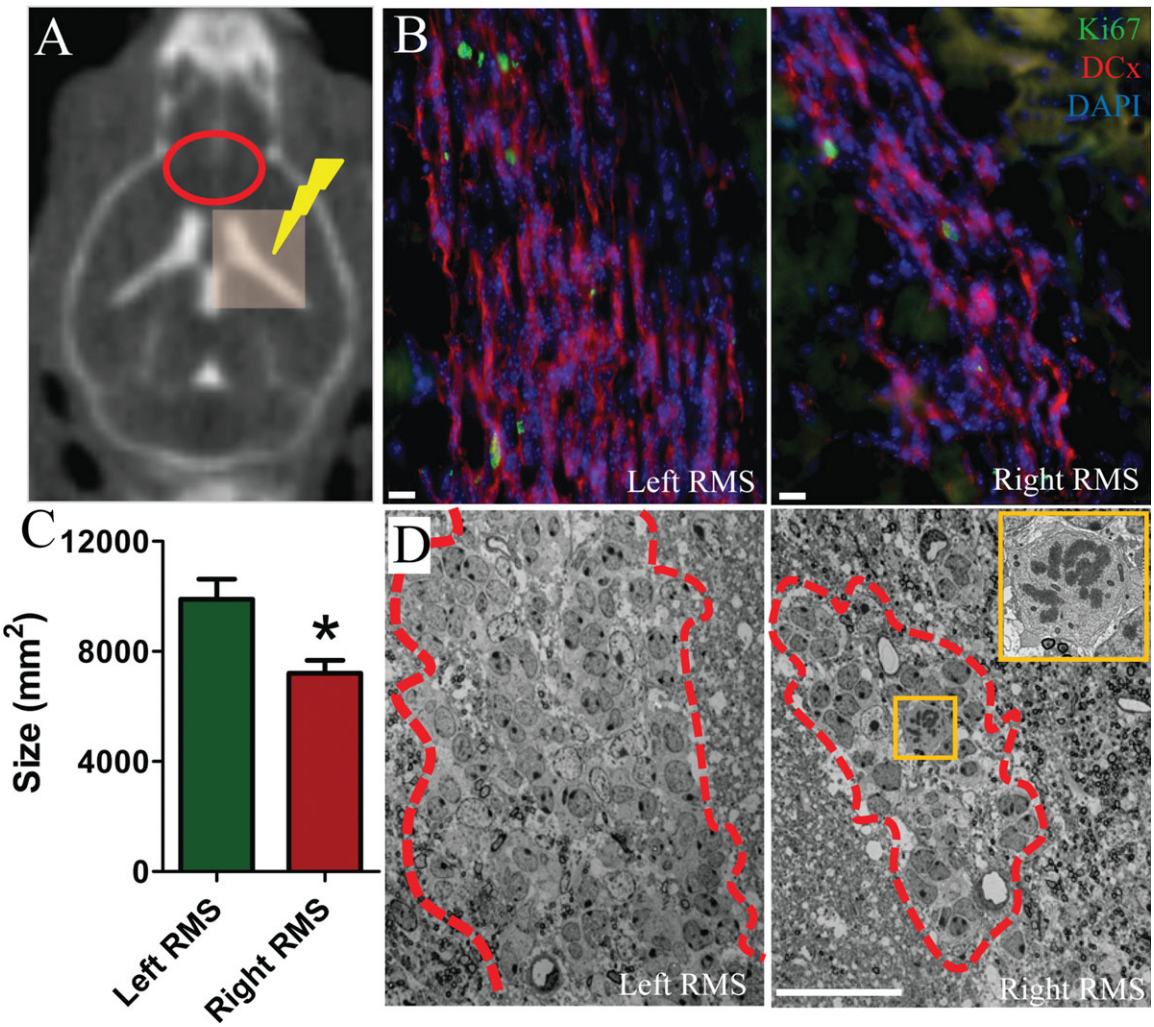

Figure 5. Fewer migrating neuroblasts were observed in the RMS of the irradiated hemisphere after 1 month. **(A):** Computed tomography (CT) image of a mouse after intrathecal iodine contrast showing ventricles and radiation plan with 3×3 mm^2 beam covering the right ventricle. Red oval shows the region of RMS on CT. **(B):** Ki67 (green) and DCx (red) immunolabeling in the RMS. Note a smaller number of migrating neuroblasts (DCx$^+$/red cells) in the right RMS compared to the left RMS. **(C):** Bar graph showing a significant reduction in the size of the RMS in the irradiated right hemisphere. **(D):** Panoramic images of migratory chains and astrocytes forming the RMS (outlined with dashed line) under electron microscope. Note the difference of the RMS size. Inset shows a neuroblast in mitotic phase at higher magnification in the right RMS. Scale bars = 10 μm (B), 20 nm (D). *, $p < .001$. Abbreviations: DAPI, 4',6-diamidino-2-phenylindole; DCx, doublecortin; RMS, rostral migratory stream.

after radiation [8, 9, 11, 36–38]. The antiproliferative effects last for several months after a single radiation treatment and are dose-dependent [9, 11, 37–39]. Most studies to date have been restricted to irradiating relatively large areas of the brain [7, 10, 39]. Very few studies used localized brain irradiation using custom-designed radiation shields or the Gamma Knife unit (Elekta Inc., Sweden) to irradiate subregions of the brain [9, 40–42]. We used SARRP technology, capable of delivering millimeter-scale beams to the mouse brain under CT guidance. This novel technology accurately mimics clinical radiation treatment, on the murine scale [31]. The localized radiation treatment used in our study is validated by immunohistochemistry against γH2Ax, a marker for DNA strand breaks [43]. Localized irradiation of right SVZ affected the proliferation in that region but not in the RMS and OB, further confirming the precise nature of the SARRP technology. There was a significant decrease in the proliferative population of cells, including NPCs and neuroblasts [24, 44], in the SVZ 1 day after localized radiation. The same effect was noticed even 1 month after localized radiation of SVZ (Fig. 1D, 1E). The decrease in the proliferative population after irradiation appeared to be due to the loss of NPCs and neuroblasts as shown by immunohistochemistry (Fig. 2B, 2C). To determine whether this was not due to changes in antibody binding efficiency, we used electron microscopy. The ultrastructural analyses from electron microscopy confirmed the elimination of NPCs and neuroblasts and the presence of NSCs in the SVZ after localized radiation. This could be explained by the quiescent nature of NSCs (cell cycle time $\sim$ 15 days) [44, 45]. Proliferating cells such as NPCs (cell cycle time $\sim$ 13 hours) and migrating neuroblasts are highly susceptible to ionizing radiation [9–11, 44, 45]. Our results on the depletion of NPCs and neuroblasts after radiation treatment are similar to the effects of antimitotic drugs such as cytosine-β-D-arabinofuranoside (AraC) [44] or the alkylating reagent *N*-ethyl-*N*-nitrosourea (ENU) on SVZ [46, 47]. The NPCs and neuroblasts regenerate from NSCs and replenish the entire SVZ in approximately 4 days after AraC treatment [44, 45]. In case of ENU-exposure, residual NSCs allowed a partial recovery after treatment [46, 47]. On the contrary, we

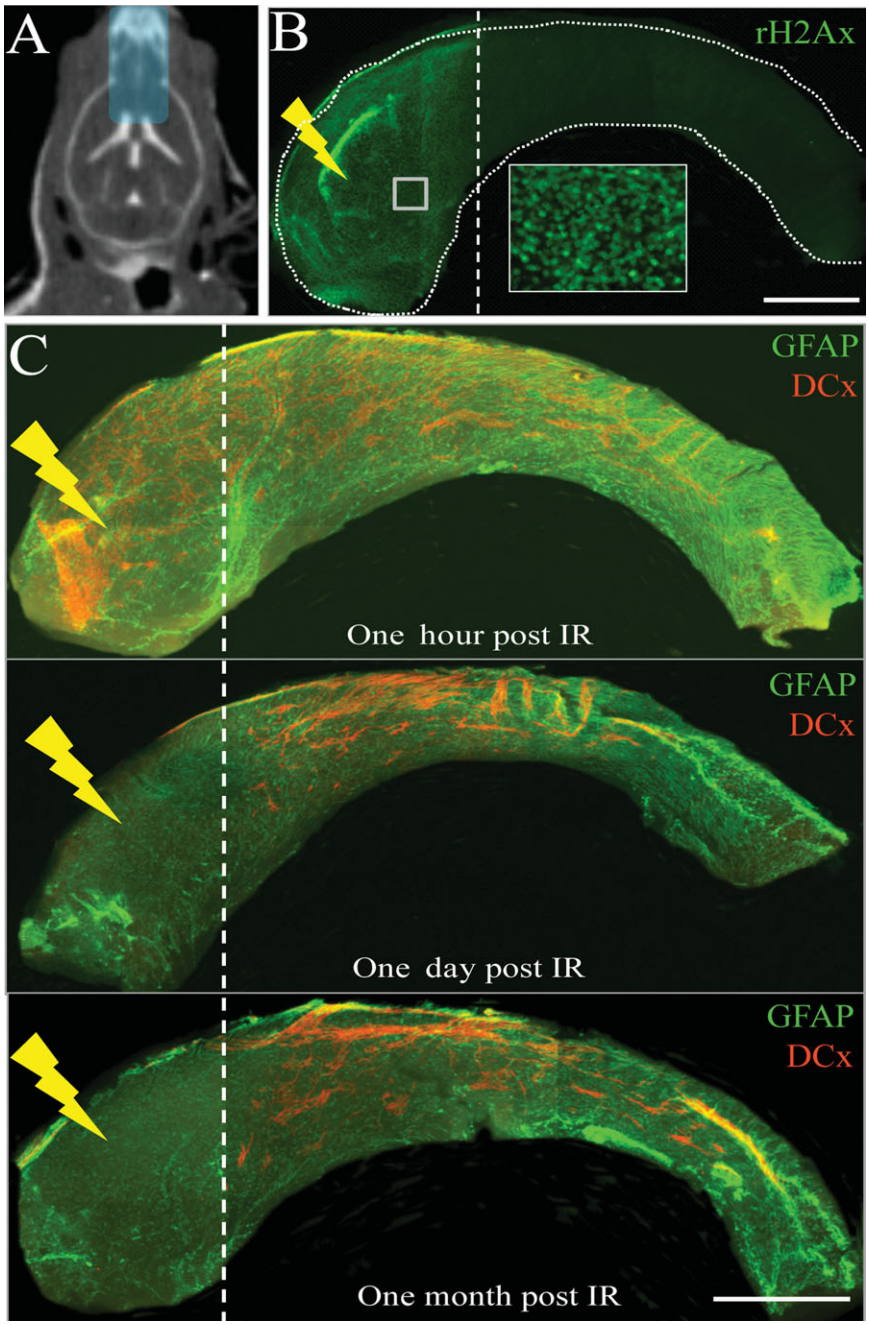

Figure 6. Neuroblasts from the posterior subventricular zone (SVZ) do not migrate into the irradiated anterior SVZ. **(A):** Computed tomography image of a mouse after intrathecal iodine contrast showing ventricles and treatment plan of 5 × 9 mm^2 beam to irradiate anterior SVZ, rostral migratory stream, and olfactory bulb. **(B):** γH2Ax staining (green) of whole mount SVZ 1 hour post-irradiation validates the localized radiation treatment plan. Inset shows the $\gamma H2Ax^+$ cells at higher magnification. **(C):** GFAP (green) and DCx (red) double labeling of SVZ whole mounts 1 hour, 1 day, and 1 month after irradiation. Scale bars = 1 mm (B, C). Abbreviations: DCx, doublecortin; GFAP, glial fibrillary acidic protein.

did not observe the regeneration of NPCs and neuroblasts from NSCs even 1 month after localized radiation of SVZ in our study (Figs. 2, 3). This suggests that irradiation might have caused permanent damage to the NSCs and/or the microenvironment that supports the proliferation and maintenance of the NSCs [10, 48–52].

NSCs are known to associate closely with the vascular niche in the SVZ [50–52]. At higher doses of irradiation, the endothelial cells that support NSCs undergo apoptosis, resulting in vascular damage and decreased neurogenesis [53–55]. We did not notice any morphological changes in endothelial cells after localized irradiation, as shown by CD31 immunohistochemistry and electron microscopy. There was no difference in the number or size of blood vessels in the irradiated SVZ as compared to the unirradiated SVZ (supporting information Fig. S1). Furthermore, the radiation dose used in our study is less than that which has been shown to cause such vascular damage [49, 56]. Therefore, the inability of NSCs to give rise to NPCs cannot be attributed to vascular niche damage. However, we cannot rule out the possibility that, even though the gross morphology of endothelial cells is intact, the molecular signals that trigger NSCs to proliferate and give

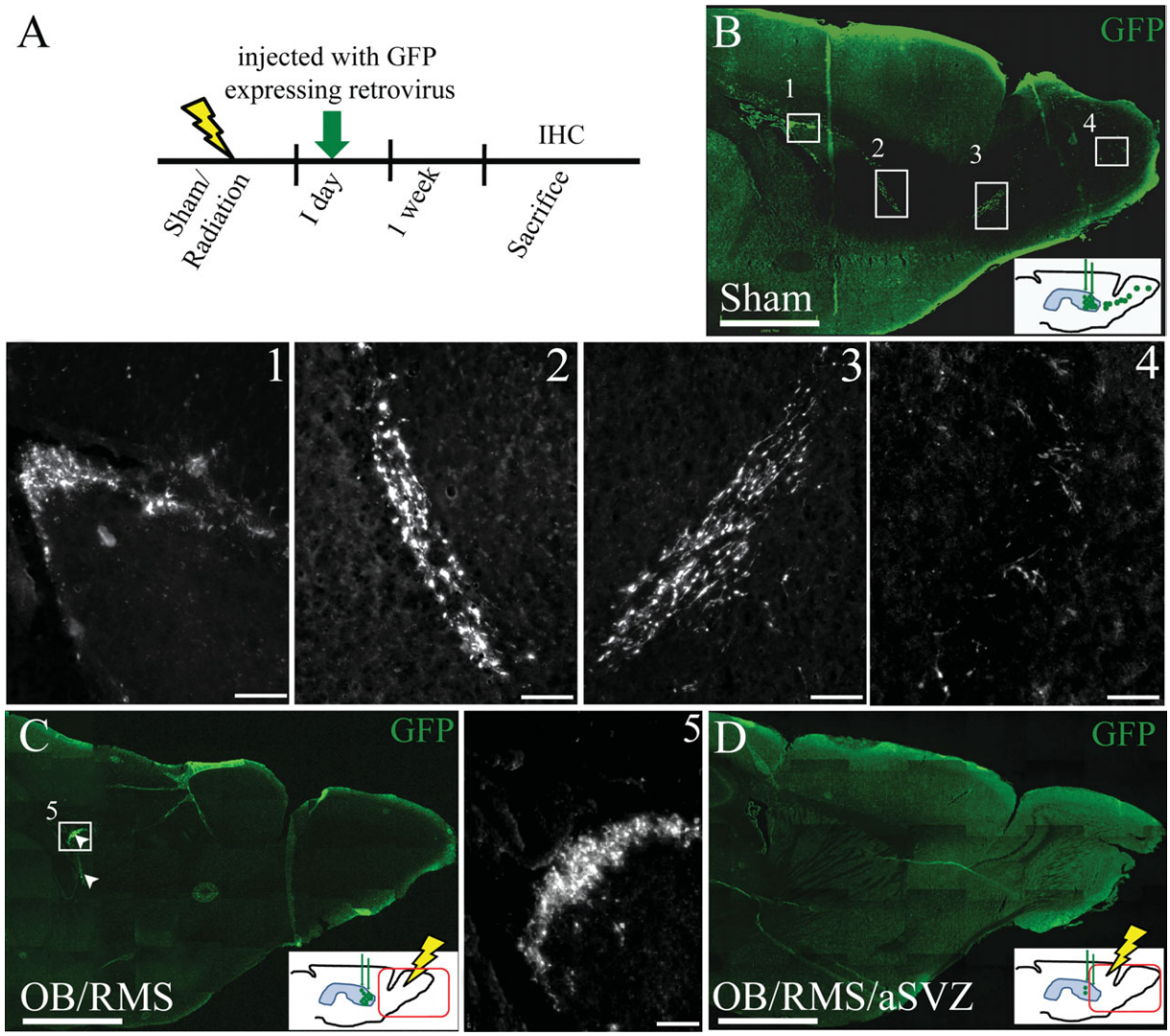

Figure 7. Neuroblasts failed to migrate through the irradiated RMS to the OB. **(A):** Experimental paradigm showing the time line for radiation, GFP expressing retroviral injections (green arrow), and sacrifice. **(B):** Sagittal section of a nonirradiated mouse brain injected with GFP expressing retrovirus into the SVZ a week after injections, insets show the GFP-labeled cells (green) in SVZ (1), descending limb of RMS (2), ascending limb of RMS (3), and OB (4) at higher magnification. **(C):** Sagittal section of a RMS/OB-irradiated mouse brain with GFP-labeled cells (green, shown in arrowheads) in SVZ (inset 5 at higher magnification) and no GFP-labeled cells in the RMS+OB. The GFP^+ cells in the SVZ appeared to be similar to the sham-irradiated mice (insets 1 and 5). **(D):** Sagittal section of a aSVZ/RMS/OB-irradiated mouse brain with no GFP-labeled cells in aSVZ/RMS/OB. Hypothetical presence of GFP^+ cells in the SVZ, RMS, and OB, a week after retroviral injections, in three different groups of mice that received sham or RMS/OB or aSVZ/RMS/OB radiation are shown in the insets of (B), (C), and (D). Scale bars = 1 mm (B--D), 100 μm (1–5). Abbreviations: GFP, green fluorescent protein; IHC, immunohistochemistry; OB, olfactory bulb; RMS, rostral migratory stream; SVZ, subventricular zone.

rise to NPCs could be affected by irradiation [57–59]. Basal lamina in the neurogenic niche is known to play a role in the proliferation of NSCs [52]. There were no differences in the ultrastructural features of basal lamina between the irradiated and nonirradiated hemispheres. However, we found it more often and extensive in the irradiated right SVZ compared to left SVZ (Fig. 3F). The extensive basal lamina observed in our animals could be a response due to the cell loss post-irradiation. Cranial irradiation is known to disrupt the microenvironment and to activate reactive microglia, affecting neurogenesis [10, 48, 49, 60]. When NSCs isolated from irradiated brain were transplanted into normal brain, NSCs regained the ability to proliferate and gave rise to neuronal and glial cell lineages [10]. In our study, we isolated cells from the irradiated and unirradiated SVZ and cultured them in NSC growth medium. While cells from irradiated SVZ remained as single cells, the cells from unirradiated SVZ divided and gave rise to neurospheres, nonadherent clusters of cells generated from NSCs in vitro [61] (Fig. 4C). Although the specific phenomena are not completely understood, our interpretation of these data is that immediately following irradiation, the rapidly dividing NPCs and migrating neuroblasts are eliminated and the NSC compartment becomes unable to fully repopulate. To better understand the effects of localized radiation on SVZ neurogenesis, detailed analysis of gene expression and/or molecular signaling pathways is warranted [62].

The ability of NPCs and neuroblasts to migrate to the site of damage and to participate in repair is well-documented [63–65]. Radiation may compromise this ability, since radiation kills NPCs and neuroblasts in the SVZ and also inflicts

long-term damage to the NSCs in this region, as shown in this and previous studies [9–11, 37–39, 41, 60, 66]. Furthermore, we show that there are fewer neuroblasts in the right RMS 1 month after irradiating the right SVZ (Fig. 5). The few neuroblasts observed in the right RMS could have been generated locally from the multipotent, self-renewing NSCs present in the RMS that were not affected by SVZ irradiation (Fig. 1F) [67–69]. The depletion of migrating neuroblasts in the right SVZ after radiation also resulted in the reduction in the size of the right RMS, suggesting that the NSCs within the RMS does not compensate for the loss of migrating neuroblasts from the SVZ and also the number of neuroblasts generated in the SVZ can affect the size of the RMS [70, 71].

With recent advancements in clinical radiotherapy planning and delivery, neurogenic niches can be spared from radiation without compromising dose coverage of the tumor [29, 30]. We have recently shown that it is possible to spare the NSC niche during radiation therapy in a retrospective clinical radiation treatment planning study [30]. NSCs may be used either to inhibit tumors by causing apoptosis or to repair tissue damage that results from radiation treatment [16–19, 65, 72]. Both uses rely on the migration of the neuroblasts to locations where they are needed, but very little is known about the effect of radiation on the migration of neuroblasts.

The anterior SVZ is one of the hotspots in the adult mouse brain with the highest number of NSC clusters [24]. When the anterior SVZ was irradiated, we noticed that neuroblasts from the posterior SVZ did not migrate through the irradiated area (Fig. 6). Even when a part of the anterior dorsal SVZ received a radiation beam as small as 1 mm in diameter, neuroblasts did not migrate through the irradiated region of the SVZ (supporting information Fig. S2). This is important in the context of emerging studies on the transplantation of modified stem cells into the mouse brain to migrate and undergo repair at the site of damage [17, 19, 65, 70]. To further confirm these findings, we labeled NSCs locally in the SVZ with GFP-expressing retrovirus 1 day after irradiation of RMS/OB or SVZ/RMS/OB. The inclusion of RMS/OB irradiation allowed us to study the effect of radiation on the migrating neuroblasts when the SVZ is spared from irradiation. The GFP-expressing cells from the SVZ failed to migrate through the RMS in the RMS/OB-irradiated mice, indicating that neuroblasts did not follow their normal migratory path through the irradiated SVZ-RMS-OB route (Fig. 7). This migratory alteration is probably not due to an intrinsic disruption in the migratory machinery of new-formed neuroblasts, but rather due to a disturbance of parenchymal migratory signaling in situ [59, 73–78]. To our knowledge, this is the first report showing a strong inhibitory effect on the migration of neuroblasts after localized radiation. The mechanisms involved in this effect are unknown. At this point, we cannot predict if this inhibitory effect on neuroblast migration after irradiation will be seen outside the SVZ-RMS-OB migration route. Also, we cannot disregard the possibility that the effect of RMS/OB irradiation would have functional impact on the SVZ, despite the proliferation in the SVZ was not compromised in these mice compared to sham mice. Although our data on the effects of localized radiation on SVZ NSCs, NPCs, and neuroblast migration are striking, much more work is needed before the mechanisms are fully understood and the clinical implications of the use of NSCs for damage repair in brain tumor patients can be fully appreciated.

Conclusions

In summary, we show that (a) SVZ-restricted irradiation affects the proliferation of type C and A cells in a highly localized manner; (b) the residual type B cells lack the ability to regenerate NPCs, which in turn give rise to migrating neuroblasts; (c) SVZ-restricted irradiation reduces the size of the RMS; and (d) neuroblasts failed to migrate through the irradiated regions of the SVZ-RMS-OB route. Future studies are indicated to investigate the effects of localized radiation not only on the molecular signals involved in the proliferation of NSCs/NPCs but also on those involved in neuroblast migration. This will allow for a thorough understanding of the effects of localized irradiation on the neurogenic regions of the brain both at the cellular and molecular levels to better improve radiotherapy protocols in the clinical setting.

Acknowledgments

This research was supported by the Maryland Stem Cell Research Fund (A.Q.H.), The Robert Wood Johnson Foundation (A.Q.H.), The Howard Hughes Medical Institute (A.Q.H.), and The National Institutes of Health (A.Q.H.). Dr. Oscar Gonzalez-Perez was supported in part by the Consejo Nacional de Ciencia y Tecnologia's grant (CONACyT, CB-2008-101476)) and Dr. Jose Manuel Garcia-Verdugo by the Prometeo grant (GVPROMETEO-2009/011). We thank Dr. Zaman Mirzadeh for technical help with whole mount dissections. We thank Dr. Michael Bonaguidi for fruitful discussions on the experimental design and data interpretation. We thank Dr. Hugo Guerrero-Cazares for helpful technical hints and critical reading of manuscript. E.F. is currently affiliated with the Department of Radiation Oncology, University of Washington Medical Center, Seattle, Washington, DC.

Disclosure of Potential Conflicts of Interest

The authors indicate no potential conflicts of interest.

References

1 Stupp R, Hegi ME, Mason WP et al. Effects of radiotherapy with concomitant and adjuvant temozolomide versus radiotherapy alone on survival in glioblastoma in a randomised phase III study: 5-year analysis of the EORTC-NCIC trial. Lancet Oncol 2009;10:459–466.

2 Stupp R, Mason WP, van den Bent MJ et al. Radiotherapy plus concomitant and adjuvant temozolomide for glioblastoma. N Engl J Med 2005;352:987–996.

3 Calabrese P, Schlegel U. Neurotoxicity of treatment. Recent Results Cancer Res 2009;171:165–174.

4 Marazziti D, Baroni S, Catena-Dell'osso M et al. Cognitive, psychological and psychiatric effects of ionizing radiation exposure. Curr Med Chem 2012;19:1864–1869

5 Silber JH, Radcliffe J, Peckham V et al. Whole-brain irradiation and decline in intelligence: The influence of dose and age on IQ score. J Clin Oncol 1992;10:1390–1396.

6 Walter AW, Mulhern RK, Gajjar A et al. Survival and neurodevelopmental outcome of young children with medulloblastoma at St Jude Children's Research Hospital. J Clin Oncol 1999;17:3720–3728.

7 Achanta P, Fuss M, Martinez JL, Jr. Ionizing radiation impairs the formation of trace fear memories and reduces hippocampal neurogenesis. Behav Neurosci 2009;123:1036–1045.

8 Fike JR, Rola R, Limoli CL. Radiation response of neural precursor cells. Neurosurg Clin N Am 2007;18:115–127, x.
9 McGinn MJ, Sun D, Colello RJ. Utilizing X-irradiation to selectively eliminate neural stem/progenitor cells from neurogenic regions of the mammalian brain. J Neurosci Methods 2008;170:9–15.
10 Monje ML, Mizumatsu S, Fike JR et al. Irradiation induces neural precursor-cell dysfunction. Nat Med 2002;8:955–962.
11 Tada E, Yang C, Gobbel GT et al. Long-term impairment of subependymal repopulation following damage by ionizing irradiation. Exp Neurol 1999;160:66–77.
12 Abrous DN, Koehl M, Le Moal M. Adult neurogenesis: From precursors to network and physiology. Physiol Rev 2005;85:523–569.
13 Alvarez-Buylla A, Garcia-Verdugo JM. Neurogenesis in adult subventricular zone. J Neurosci 2002;22:629–634.
14 Ming GL, Song H. Adult neurogenesis in the mammalian central nervous system. Annu Rev Neurosci 2005;28:223–250.
15 Menn B, Garcia-Verdugo JM, Yaschine C et al. Origin of oligodendrocytes in the subventricular zone of the adult brain. J Neurosci 2006;26:7907–7918.
16 Glass R, Synowitz M, Kronenberg G et al. Glioblastoma-induced attraction of endogenous neural precursor cells is associated with improved survival. J Neurosci 2005;25:2637–2646.
17 Aboody KS, Brown A, Rainov NG et al. Neural stem cells display extensive tropism for pathology in adult brain: Evidence from intracranial gliomas. Proc Natl Acad Sci USA 2000;97:12846–12851.
18 Achanta P, Sedora Roman NI, Quinones-Hinojosa A. Gliomagenesis and the use of neural stem cells in brain tumor treatment. Anticancer Agents Med Chem 2010;10:121–130.
19 Ahmed AU, Thaci B, Alexiades NG et al. Neural stem cell-based cell carriers enhance therapeutic efficacy of an oncolytic adenovirus in an orthotopic mouse model of human glioblastoma. Mol Ther 2011;19:1714–1726.
20 Frank RT, Edmiston M, Kendall SE et al. Neural stem cells as a novel platform for tumor-specific delivery of therapeutic antibodies. PLoS One 2009;4:e8314.
21 Lee EX, Lam DH, Wu C et al. Glioma gene therapy using induced pluripotent stem cell derived neural stem cells. Mol Pharm 2011;8:1515–1524.
22 Quinones-Hinojosa A, Sanai N, Soriano-Navarro M et al. Cellular composition and cytoarchitecture of the adult human subventricular zone: A niche of neural stem cells. J Comp Neurol 2006;494:415–434.
23 Sanai N, Tramontin AD, Quinones-Hinojosa A et al. Unique astrocyte ribbon in adult human brain contains neural stem cells but lacks chain migration. Nature 2004;427:740–744.
24 Mirzadeh Z, Merkle FT, Soriano-Navarro M et al. Neural stem cells confer unique pinwheel architecture to the ventricular surface in neurogenic regions of the adult brain. Cell Stem Cell 2008;3:265–278.
25 Doetsch F, Garcia-Verdugo JM, Alvarez-Buylla A. Cellular composition and three-dimensional organization of the subventricular germinal zone in the adult mammalian brain. J Neurosci 1997;17:5046–5061.
26 Lois C, Alvarez-Buylla A. Proliferating subventricular zone cells in the adult mammalian forebrain can differentiate into neurons and glia. Proc Natl Acad Sci USA 1993;90:2074–2077.
27 Lois C, Garcia-Verdugo JM, Alvarez-Buylla A. Chain migration of neuronal precursors. Science 1996;271:978–981.
28 Curtis MA, Kam M, Nannmark U et al. Human neuroblasts migrate to the olfactory bulb via a lateral ventricular extension. Science 2007;315:1243–1249.
29 Marsh JC, Godbole R, Diaz AZ et al. Sparing of the hippocampus, limbic circuit and neural stem cell compartment during partial brain radiotherapy for glioma: A dosimetric feasibility study. J Med Imaging Radiat Oncol 2011;55:442–449.
30 Redmond KJ, Achanta P, Grossman SA et al. A radiotherapy technique to limit dose to neural progenitor cell niches without compromising tumor coverage. J Neurooncol 2011;104:579–587.
31 Wong J, Armour E, Kazanzides P et al. High-resolution, small animal radiation research platform with x-ray tomographic guidance capabilities. Int J Radiat Oncol Biol Phys 2008;71:1591–1599.
32 Ford EC, Achanta P, Purger D et al. Localized CT-guided irradiation inhibits neurogenesis in specific regions of the adult mouse brain. Radiat Res 2011;175:774–783.
33 Mirzadeh Z, Doetsch F, Sawamoto K et al. The subventricular zone en-face: Wholemount staining and ependymal flow. J Vis Exp 2010;6:1938.
34 Ferron SR, Andreu-Agullo C, Mira H et al. A combined ex/in vivo assay to detect effects of exogenously added factors in neural stem cells. Nat Protoc 2007;2:849–859.
35 Ge S, Goh EL, Sailor KA et al. GABA regulates synaptic integration of newly generated neurons in the adult brain. Nature 2006;439:589–593.
36 Belvindrah R, Lazarini F, Lledo PM. Postnatal neurogenesis: From neuroblast migration to neuronal integration. Rev Neurosci 2009;20:331–346.
37 Hellstrom NA, Bjork-Eriksson T, Blomgren K et al. Differential recovery of neural stem cells in the subventricular zone and dentate gyrus after ionizing radiation. Stem Cells 2009;27:634–641.
38 Panagiotakos G, Alshamy G, Chan B et al. Long-term impact of radiation on the stem cell and oligodendrocyte precursors in the brain. PLoS One 2007;2:e588.
39 Tada E, Parent JM, Lowenstein DH et al. X-irradiation causes a prolonged reduction in cell proliferation in the dentate gyrus of adult rats. Neuroscience 2000;99:33–41.
40 Shi L, Molina DP, Robbins ME et al. Hippocampal neuron number is unchanged 1 year after fractionated whole-brain irradiation at middle age. Int J Radiat Oncol Biol Phys 2008;71:526–532.
41 Jirak D, Namestkova K, Herynek V et al. Lesion evolution after gamma knife irradiation observed by magnetic resonance imaging. Int J Radiat Biol 2007;83:237–244.
42 Santarelli L, Saxe M, Gross C et al. Requirement of hippocampal neurogenesis for the behavioral effects of antidepressants. Science 2003;301:805–809.
43 Saxe MD, Battaglia F, Wang JW et al. Ablation of hippocampal neurogenesis impairs contextual fear conditioning and synaptic plasticity in the dentate gyrus. Proc Natl Acad Sci USA 2006;103:17501–17506.
44 Rogakou EP, Nieves-Neira W, Boon C et al. Initiation of DNA fragmentation during apoptosis induces phosphorylation of H2AX histone at serine 139. J Biol Chem 2000;275:9390–9395.
45 Doetsch F, Caille I, Lim DA et al. Subventricular zone astrocytes are neural stem cells in the adult mammalian brain. Cell 1999;97:703–716.
46 Morshead CM, Craig CG, van der Kooy D. In vivo clonal analyses reveal the properties of endogenous neural stem cell proliferation in the adult mammalian forebrain. Development 1998;125:2251–2261.
47 Capilla-Gonzalez V, Gil-Perotin S, Ferragud A et al. Exposure to N-ethyl-N-nitrosourea in adult mice alters structural and functional integrity of neurogenic sites. PLoS One 2012;7:e29891.
48 Capilla-Gonzalez V, Gil-Perotin S, Garcia-Verdugo JM. Postnatal exposure to N-ethyl-N-nitrosurea disrupts the subventricular zone in adult rodents. Eur J Neurosci 2010;32:1789–1799.
49 Snyder EY, Park KI. Limitations in brain repair. Nat Med 2002;8:928–930.
50 Monje ML, Palmer T. Radiation injury and neurogenesis. Curr Opin Neurol 2003;16:129–134.
51 Shen Q, Goderie SK, Jin L et al. Endothelial cells stimulate self-renewal and expand neurogenesis of neural stem cells. Science 2004;304:1338–1340.
52 Shen Q, Wang Y, Kokovay E et al. Adult SVZ stem cells lie in a vascular niche: A quantitative analysis of niche cell-cell interactions. Cell Stem Cell 2008;3:289–300.
53 Tavazoie M, Van der Veken L, Silva-Vargas V et al. A specialized vascular niche for adult neural stem cells. Cell Stem Cell 2008;3:279–288.
54 Brown WR, Thore CR, Moody DM et al. Vascular damage after fractionated whole-brain irradiation in rats. Radiat Res 2005;164:662–668.
55 Li YQ, Chen P, Haimovitz-Friedman A et al. Endothelial apoptosis initiates acute blood-brain barrier disruption after ionizing radiation. Cancer Res 2003;63:5950–5956.
56 Ljubimova NV, Levitman MK, Plotnikova ED et al. Endothelial cell population dynamics in rat brain after local irradiation. Br J Radiol 1991;64:934–940.
57 Otsuka S, Coderre JA, Micca PL et al. Depletion of neural precursor cells after local brain irradiation is due to radiation dose to the parenchyma, not the vasculature. Radiat Res 2006;165:582–591.
58 Andreu-Agullo C, Morante-Redolat JM, Delgado AC et al. Vascular niche factor PEDF modulates Notch-dependent stemness in the adult subependymal zone. Nat Neurosci 2009;12:1514–1523.
59 Ramirez-Castillejo C, Sanchez-Sanchez F, Andreu-Agullo C et al. Pigment epithelium-derived factor is a niche signal for neural stem cell renewal. Nat Neurosci 2006;9:331–339.
60 Wittko IM, Schanzer A, Kuzmichev A et al. VEGFR-1 regulates adult olfactory bulb neurogenesis and migration of neural progenitors in the rostral migratory stream in vivo. J Neurosci 2009;29:8704–8714.
61 Monje ML, Toda H, Palmer TD. Inflammatory blockade restores adult hippocampal neurogenesis. Science 2003;302:1760–1765.
62 Reynolds BA, Weiss S. Generation of neurons and astrocytes from isolated cells of the adult mammalian central nervous system. Science 1992;255:1707–1710.
63 Mu Y, Lee SW, Gage FH. Signaling in adult neurogenesis. Curr Opin Neurol 2010;20:416–423.
64 Arvidsson A, Collin T, Kirik D et al. Neuronal replacement from endogenous precursors in the adult brain after stroke. Nat Med 2002;8:963–970.

65 Goings GE, Sahni V, Szele FG. Migration patterns of subventricular zone cells in adult mice change after cerebral cortex injury. Brain Res 2004;996:213–226.
66 Aboody K, Capela A, Niazi N et al. Translating stem cell studies to the clinic for CNS repair: Current state of the art and the need for a Rosetta Stone. Neuron 2011;70:597–613.
67 Rola R, Raber J, Rizk A et al. Radiation-induced impairment of hippocampal neurogenesis is associated with cognitive deficits in young mice. Exp Neurol 2004;188:316–330.
68 Craig CG, D'sa R, Morshead CM et al. Migrational analysis of the constitutively proliferating subependyma population in adult mouse forebrain. Neuroscience 1999;93:1197–1206.
69 Gritti A, Bonfanti L, Doetsch F et al. Multipotent neural stem cells reside into the rostral extension and olfactory bulb of adult rodents. J Neurosci 2002;22:437–445.
70 Hack MA, Saghatelyan A, de Chevigny A et al. Neuronal fate determinants of adult olfactory bulb neurogenesis. Nat Neurosci 2005;8: 865–872.
71 Diaz D, Recio JS, Baltanas FC et al. Long-lasting changes in the anatomy of the olfactory bulb after ionizing irradiation and bone marrow transplantation. Neuroscience 2011;173:190–205.
72 Martoncikova M, Racekova E, Orendacova J. The number of proliferating cells in the rostral migratory stream of rat during the first postnatal month. Cell Mol Neurobiol 2006;26:1453–1461.
73 Hallbergson AF, Gnatenco C, Peterson DA. Neurogenesis and brain injury: Managing a renewable resource for repair. J Clin Invest 2003; 112:1128–1133.
74 Catchpole T, Henkemeyer M. EphB2 tyrosine kinase-dependent forward signaling in migration of neuronal progenitors that populate and form a distinct region of the dentate niche. J Neurosci 2011;31: 11472–11483.
75 Connor B, Gordon RJ, Jones KS et al. Deviating from the well travelled path: Precursor cell migration in the pathological adult mammalian brain. J Cell Biochem 2011;112:1467–1474.
76 Kaneko N, Marin O, Koike M et al. New neurons clear the path of astrocytic processes for their rapid migration in the adult brain. Neuron 2010;67:213–223.
77 Nie K, Molnar Z, Szele FG. Proliferation but not migration is associated with blood vessels during development of the rostral migratory stream. Dev Neurosci 2010;32:163–172.
78 Wang Y, Kaneko N, Asai N et al. Girdin is an intrinsic regulator of neuroblast chain migration in the rostral migratory stream of the postnatal brain. J Neurosci 2011;31:8109–8122.


See www.StemCells.com for supporting information available online.